Molecular Crystals and Liquid Crystals

Publication details, including instructions for authors and subscription information:
http://www.tandfonline.com/loi/gmcl20

Gap Material Study for Holographically Formed Polymer Dispersed Liquid Crystal Composite Film Stacks

Anna E. Fox [a], Marie Cosgrove-Davies [a] & Adam K. Fontecchio [a]

[a] Department of Electrical and Computer Engineering, Drexel University, Philadelphia, PA, USA

Version of record first published: 22 Sep 2010

To cite this article: Anna E. Fox, Marie Cosgrove-Davies & Adam K. Fontecchio (2007): Gap Material Study for Holographically Formed Polymer Dispersed Liquid Crystal Composite Film Stacks, Molecular Crystals and Liquid Crystals, 478:1, 151/[907]-162/[918]

To link to this article: http://dx.doi.org/10.1080/15421400701735657

Mol. Cryst. Liq. Cryst., Vol. 478, pp. 151/[907]–162/[918], 2007

ISSN: 1542-1406 print/1563-5287 online
DOI: 10.1080/15421400701735657

Gap Material Study for Holographically Formed Polymer Dispersed Liquid Crystal Composite Film Stacks

Anna E. Fox
Marie Cosgrove-Davies
Adam K. Fontecchio
Department of Electrical and Computer Engineering,
Drexel University, Philadelphia, PA, USA

We present a comparison of materials for adhering layers of holographically formed polymer dispersed liquid crystal (H-PDLC) films layered in stacks fabricated on common substrates. The results of this study are used in applications that rely on maximization of transmitted light through the layers of H-PDLC. Data is presented by comparing a simulated transmission envelope modeled on the individual H-PDLC cells with the actual stacked transmission spectrum. Additionally, data is presented on the quality of the wavefront of H-PDLC transmission spectrum individually and layered using air and index matching layers.

Keywords: H-PDLC; H-PDLC stacks; H-PDLC wavefront; optical adhesive

I. INTRODUCTION

Holographically formed polymer dispersed liquid crystal (H-PDLC) films are materials consisting of spherical liquid crystal droplets arranged within a firm polymer matrix. This type of film is phase separated when exposed to an interference pattern causing the photosensitive monomer to polymerize in the bright fringes and liquid crystal to migrate to the dark regions [1]. Once phase separation has occurred, the resulting periodic pattern is known as a Bragg grating. The structure is permanent and possesses unique optical properties

The authors wish to thank the NASA New Investigator Program (Grant #NNG04G042G), the NSF-REU Program (Grant #0552711) and the NSF Graduate Research Fellowship Program.

Address correspondence to Adam K. Fontecchio, Department of Electrical and Computer Engineering, Drexel University, PA 19104, Philadelphia, PA, USA. E-mail: fontecchio@drexel.edu

[2]. There exists a refractive index mismatch between layers of liquid crystal and polymer due to random rotational alignment of the liquid crystal droplets with respect to the direction of their director vector. The resulting Bragg reflection occurs and is governed by the equation

$$\Lambda = \frac{\lambda}{2n\sin(\theta)}$$

where Λ is the grating pitch, n is the average index of refraction, λ is the wavelength of the exposure beam, and θ is the angle at which the beams interfere. Figure 1(a) illustrates this effect.

Application of a bias will cause the nematic director in the liquid crystal droplets to align in the direction of the field. Due to the anisotropy of the material, the average refractive index will change and match that of the polymer matrix as the director rotates. The Bragg reflection is suppressed and the material becomes transparent. Figure 1(b) illustrates the change in liquid crystal orientation with the application of bias. Removal of bias will allow the directors to return to their original state of random rotational alignment and the Bragg reflection returns.

H-PDLC Bragg gratings have been characterized and reported on in reflection and transmission modes. This material has emerging applications in fields related to display technology including conformal [3] and reflective displays [4,5], photonic bandgap materials applications

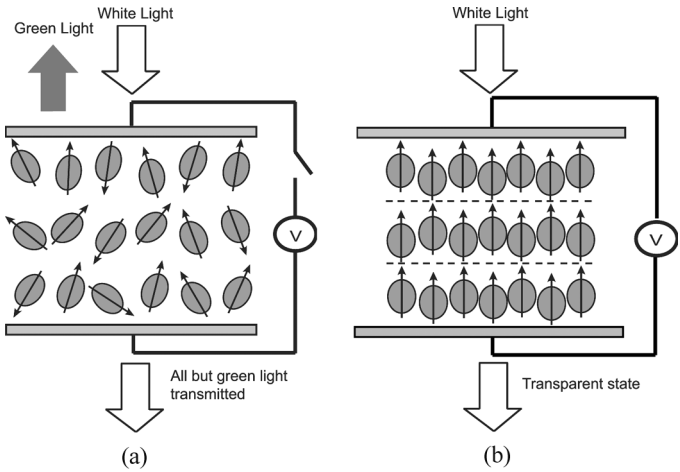

FIGURE 1 (a) Liquid crystal droplets in random orientation showing a green reflection. (b) Liquid crystal droplets aligning with applied bias.

including lasing [6] and DFB lasing [7]. Stacking layers of H-PDLC material has been reported to have applications in reflective display technology [8], improving display reflectance [9], and reflection mode spectroscopy [10].

Applications such as a transmission-mode thin film spectrometer rely on maximum transmission through the layers of H-PDLC for functionality, therefore a study to determine which index matching fluid/optical adhesive maximizes transmission through multiple H-PDLC layers was performed. H-PDLC samples on anti-reflection (AR) and indium-tin-oxide (ITO) coated Corning 1737 glass were individually characterized for transmission, then stacked with an index matching fluid. The transmission characteristics of the stack of two were measured and compared with a model based on the individual H-PDLC transmission characteristics. This was repeated for samples formed on ITO coated Corning 1737 glass without AR coating to determine the effect of an AR coating on the index matching fluid that maximizes transmission. Index matching fluids/optical adhesives sampled were Norland Optical Adhesive NOA65 (Norland, Inc.), NOA68 (Norland, Inc.), NOA71 (Norland, Inc.), and air for comparison.

In addition to quantifying transmission loss through layers of H-PDLC with different index matching fluid, analysis of transmitted wavefront quality was performed using a Shack-Hartmann wavefront analyzer. A Shack-Hartmann style wavefront analyzer measures the displacement of a series of focal spots produced when the incident beam passes through a 2-dimensional lens array. The derivative of the optical difference determined from the focal spot displacement is the wavefront slope [11]. Using this information, software analysis derives wavefront fringe pattern, Strehl ratio, Zernike polynomial fits for the wavefront, and encircled energy.

II. EXPERIMENTAL

Samples were formed using a typical acrylate mixture of tri and hexafunctional monomers 20.5% Ebecryl 8301 (UCB Chemical Corp.), 20.5% Ebecryl 4866 (UCB Chemical Corp.), 12.6% photoinitiator, 10% Tween80 surfactant (Sigma-Aldrich), and 36.4% BL038 liquid crystal (EMD Industries) [12]. The photoinitiator mixture consisted of 4% Rose Bengal (Aldrich), 10% n-phenylglycine (Aldrich), and 86% n-vinyl pyrrolidinone (Acros Organics). H-PDLC films were formed by placing a drop of syrup on both AR and non-AR coated ITO glass spaced with 5 μm spacers. Holographic exposure was performed using a two-beam method illustrated in Figure 2. A Coherent Verdi 532 nm CW laser with a power density of 66 mW/cm^2 was the

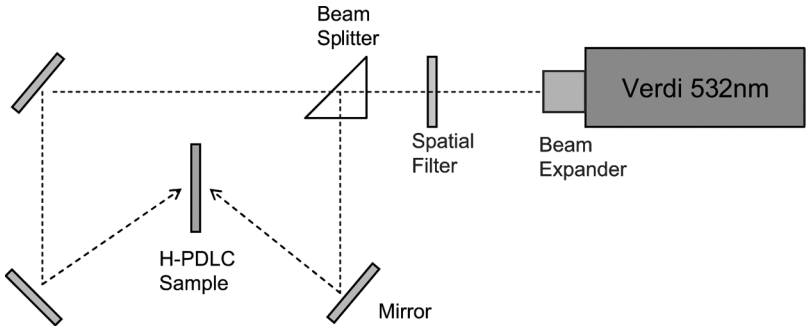

FIGURE 2 Two-beam exposure method of holographically forming H-PDLC films.

light source for exposure, and exposure time was 30 seconds. The samples were post cured with UV exposure to polymerize any remaining monomer.

Using an Ocean Optics spectrometer and white light source, a transmission spectrum was collected for each sample. Transmission measurements were calibrated using a sample of acrylate syrup without liquid crystal cured on the appropriate glass for the H-PDLC being measured. Calibrating the transmission measurement using this method allowed observation of losses due only to liquid crystal droplets and not to glass, coating, or polymer.

H-PDLC samples were paired and adhered with NOA65, NOA68, or NOA71. Samples were pressed in a balloon press prior to UV curing. The air gap stacks were prepared by placing a thin line of NOA65 on the edge of the glass. The optical adhesive acted to hold the samples in place rather than as an index matching fluid. Transmission of the stacked H-PDLC samples was remeasured and compared with an expected transmission envelope simulated using the unstacked transmission data for each individual sample.

In addition to transmission characterizations, these individual samples and stacked samples were measured for transmission wavefront quality. Using an AOA, Inc. Shack-Hartmann style wavefront analyzer, wavefront quality of the single H-PDLC transmission spectrum and the H-PDLC stack pairs were measured. To perform this analysis, a He-Ne laser was aligned as a source and calibrated to remove aberrations within the test optics. The H-PDLC under test was placed in the source path to determine the transmitted wavefront distortion. The stacks of two H-PDLC samples adhered with index matching fluids NOA65, NOA68, NOA71, and an air gap that were analyzed for transmission loss were also analyzed for transmitted wavefront quality.

III. RESULTS AND DISCUSSION

A. Transmission Analysis

Each H-PDLC sample transmission spectrum was characterized individually and the data was used to calculate the ideal predicted transmission of the stack. The actual transmission of the adhered samples was measured and compared to the ideal transmission envelope. In general, the samples fabricated on AR-ITO formed better gratings than that of non-AR ITO glass. This is due to better coupling of 532 nm light into the sample during holographic exposure. Though it was initially speculated that the AR coating would interfere with the index matching that the gap material offered, in general samples on AR-ITO had stacked transmission envelopes closer to ideal than samples formed on non-AR ITO glass. The data in Figure 3(b) indicates that the actual transmission envelope was closest to the ideal case using NOA65 as a gap-filling layer with actual transmission differing only 4.7% from the ideal case. Using NOA71, shown in Figure 3(c), measured and predicted had 7.3% difference while NOA68, shown in Figure 3(d) had 11.63% difference between actual and ideal cases. An air gap sample, shown in Figure 3a, caused 19.5% discrepancy between ideal and actual transmission efficiencies.

Examining the transmission data collected using non-AR ITO glass, shown in Figure 4, the loss was minimized using NOA65 as a gap fill and index-matching layer. The discrepancy between the ideal and actual case is 8.39%. NOA71, shown in Figure 4(c), presented a 14.07% difference while NOA68, shown in Figure 4(d), presented a 16.9% difference between ideal and actual cases. H-PDLC stacked with an air gap, shown in Figure 4(a), presented a difference between ideal and actual transmission of 20.8%.

The respective refractive indices of cured NOA65, NOA68, and NOA71 are 1.524, 1.54, and 1.56. The index of Corning 1737 is 1.5203 at 548.1 nm and the index of the ITO coating used is 1.55. It is clear that regardless of the AR and ITO coating, transmission loss is minimized between H-PDLC samples fabricated on Corning 1737 glass when stacked with NOA65, probably due to index matching of the glass substrates and the gap fill material.

B. Wavefront Analysis

In addition to determining which index matching fluid most reduces transmission loss when stacking H-PDLC layers on Corning 1737 glass, measurements were taken to determine the quality of the transmitted wavefront through a single H-PDLC sample and a stack of two

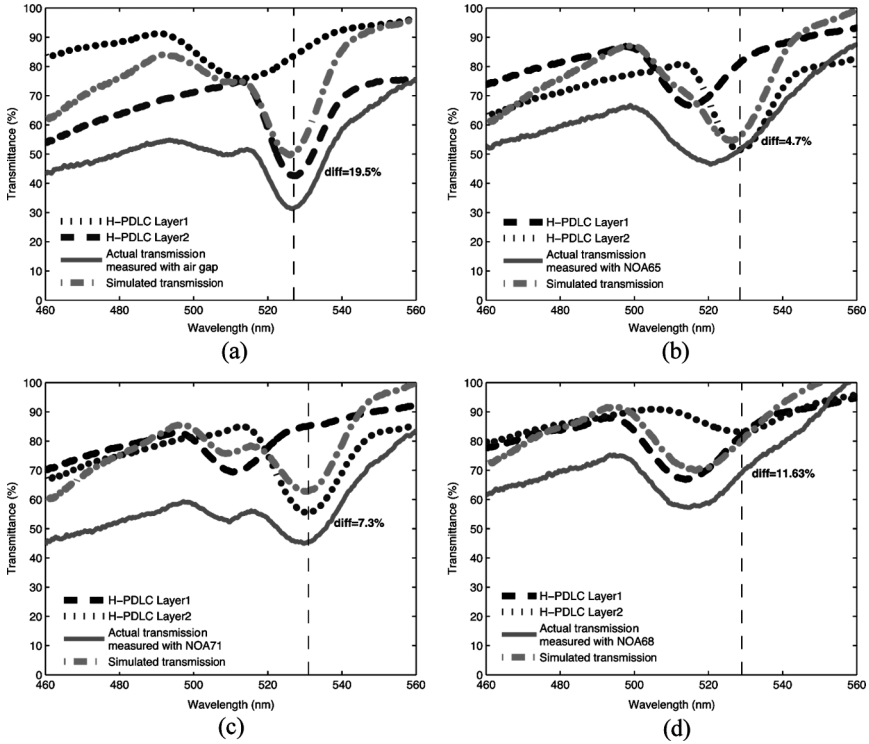

FIGURE 3 (a) Transmission data of a stack with air in between the two samples on AR ITO glass. (b) Transmission data of a stack with NOA65 as an index matching fluid on AR ITO glass. (c) Transmission data of a stack with NOA71 as an index matching fluid on AR ITO glass. (d) Transmission data of a stack with NOA68 as an index matching fluid on AR ITO glass.

H-PDLC samples. Wavefront analysis measurements were performed with a Shack-Hartmann style wavefront analyzer that functions by passing the incident beam through a 2-dimensional lenslet array. The displacement of the series of focused points from the reference points can be determined with a CCD and software analysis. Using the optical path difference, software analysis can derive the wavefront slope which yields information on Strehl ratio, Zernike polynomial fit for the wavefront, fractionalized encircled energy, fringe pattern, and a contour map of the wavefront itself [11].

Strehl ratio is the ratio of the peak intensity of an optical system's point spread function for an aberrated system compared with that of an unaberrated system [13]. Strehl ratio can be equivocated to

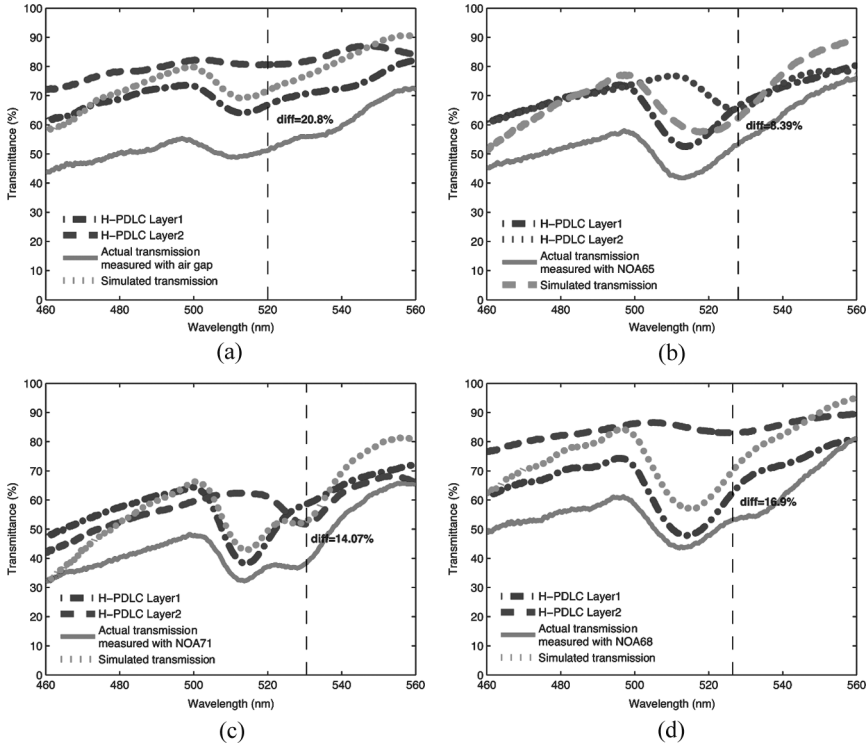

FIGURE 4 (a) Transmission data of a stack with air in between the two samples on non-AR ITO glass. (b) Transmission data of a stack with NOA65 as an index matching fluid on non-AR ITO glass. (c) Transmission data of a stack with NOA71 as an index matching fluid on AR non-ITO glass. (d) Transmission data of a stack with NOA68 as an index matching fluid on AR non-ITO glass.

wavefront quality using the Rayleigh quarter-wave rule suggesting a Strehl ratio of 0.80 has a peak-to-valley (PV) wavefront error of $\lambda/4$ [14] or by the Marechal criterion that states a Strehl ratio greater than 0.8 yields an RMS wavefront error better than $\lambda/14$ [15]. Strehl ratios measured for transmission through single H-PDLC samples averaged 0.9723 placing its wavefront quality better than a quarter-wave of PV wavefront aberration and greater than $\lambda/14$ RMS wavefront error. The average Strehl ratio of two H-PDLC samples with an air gap was 0.9491, for two H-PDLC samples with NOA65 yielded 0.9393. NOA71 and NOA68 adhered samples yielded Strehl ratios of 0.9467 and 0.9683 respectively. Strehl ratio is related to RMS wavefront error

TABLE 1 Strehl Ratio and RMS Wavefront Equivalents

Sample type	Strehl ratio	RMS wavefront error (waves)
Single	0.9723	$\lambda/37.3$
Air Gap	0.9491	$\lambda/25.5$
NOA65	0.9393	$\lambda/27.9$
NOA68	0.9683	$\lambda/35.3$
NOA71	0.9467	$\lambda/27.3$

for a point on the image plane P by

$$I(P) = 1 - \left(\frac{2\pi}{\lambda}\right)^2 (\Delta\Phi_P)^2$$

where I(P) represents Strehl ratio and $\Delta\Phi_P$ is the RMS wavefront error measured in waves [14]. Table 1 displays calculated RMS wavefront error from the Strehl ratios for each of the measured H-PDLC samples. RMS wavefront error represents the difference in wavefront quality with the addition of an H-PDLC sample with respect to a calibrated source.

The Shack-Hartmann wavefront analyzer can produce a fringe pattern, known as an interferogram, which is a qualitative measure of wavefront error [16]. Figure 5(a) is the fringe pattern generated for a single H-PDLC transmission. Figures 5(b)–(e) are fringe patterns for stacks of two H-PDLC samples adhered with air gap, NOA65, NOA71, and NOA68. A perfectly unaberrated fringe pattern has parallel fringes. The equation relating wavefront as a function of position $W(x,y)$ with the sources of primary aberration

$$W(x,y) = A(x^2+y^2) + By(x^2+y^2) + C(x^2+3y^2) + D(x^2+y^2) + Ey + Fx + G$$

where A is the coefficient representing spherical aberration, B is the coefficient for coma, C represents astigmatism, D represents defocus, E and F represent tilt in the x and y directions, and G represents piston [16]. Referring to Figure 5(a), in the fringe pattern of transmission through a single H-PDLC it is difficult to see which aberration, if any, causes wavefront distortion. In the fringe patterns for pairs of two H-PDLC samples, the fringe lines have a slight bowing towards the right of the figure. This curvature appearing in the fringe lines represents a small amount of astigmatism in all the stacked samples, and a small amount of coma in the samples adhered with NOA65 and the

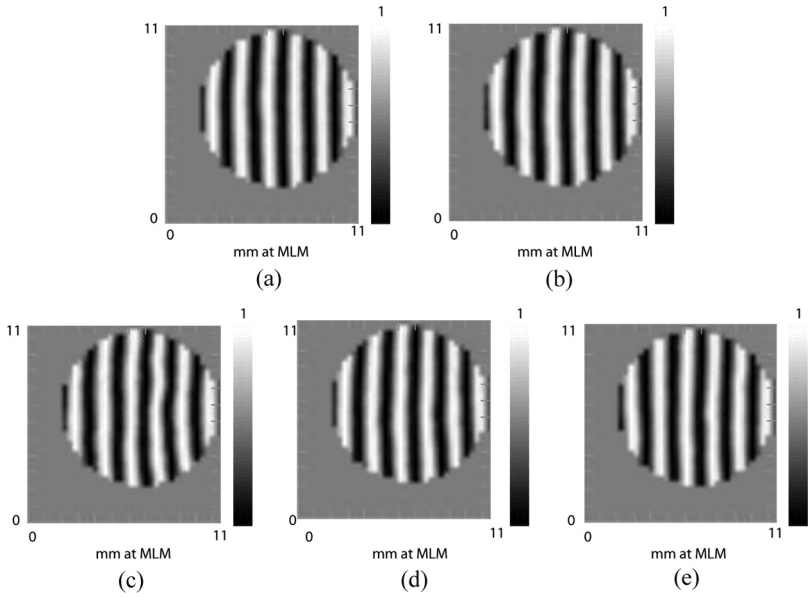

FIGURE 5 (a) Fringe pattern produced for analysis of the transmission wavefront through a single H-PDLC sample. (b) Fringe pattern for analysis of transmission wavefront propagating through two H-PDLC samples with an air gap. (c) Fringe pattern for analysis of transmission wavefront propagating through two H-PDLC samples adhered with NOA65. (d) Fringe pattern for analysis of transmission wavefront propagating through two H-PDLC samples adhered with NOA71. (e) Fringe pattern for analysis of transmission wavefront propagating through two H-PDLC samples adhered with an NOA68.

samples with an air gap. This can be confirmed with the Zernike numbers or the coefficients of primary wavefront aberration obtained for these measurements.

The Zernike values obtained for this wavefront are a polynomial fit for the coefficients that describe the wavefront. Displayed in Table 2 are the primary aberration coefficients. Clearly, all primary aberrations have a contribution to the distortion of the wavefront except defocus. In the case of transmission through the single H-PDLC sample, only 0° astigmatism has a major contribution. The primary aberration Zernike numbers collected for samples adhered with NOA65, NOA68, NOA71, and samples with an air gap are also shown in Table 2. Again, each of the primary aberrations have a presence in the transmitted wavefront distortion, except defocus, with major contributions from 0° astigmatism in all the stacked samples, contributions

TABLE 2 Primary Aberration Zernike Numbers Obtained for Transmitted Wavefront Though all H-PDLC Samples

Primary aberration	Single	Air	NOA65	NOA68	NOA71
X Tilt	−0.009806	0.000251	−0.007311	−0.001972	0.009800
Y Tilt	−0.005408	0.011237	0.010276	0.006296	0.001412
Focus	0.00000	0.00000	0.00000	0.00000	0.00000
0° Astigmatism	−0.035504	−0.046167	−0.057100	−0.027818	−0.048309
45° Astigmatism	−0.002058	0.004934	0.008659	0.020599	−0.013256
X Coma	0.007527	0.004934	0.020860	0.005706	−0.005408
Y Coma	0.008259	−0.019321	−0.015167	−0.007838	−0.006490
Spherical	0.000890	0.002188	0.011763	−0.002472	0.000495

from Y coma in the samples with an air gap, and 45° astigmatism in the samples adhered with NOA71. The H-PDLC samples adhered with NOA65 displayed the most visible aberration in its primary Zernike numbers with major contributions from 0° astigmatism, X and Y coma, and spherical aberration. Samples adhered with NOA65 also yielded the lowest Strehl ratio. Notice that the Zernike coefficient for defocus is 0. This was typical of the stack data collected.

Fractional encircled energy E within radius W, a final parameter that was collected for wavefront analysis of H-PDLC transmission is defined by the following integral

$$E(W) = K \int_0^{2\pi} \int_{\rho=0}^{W} I(\rho, \theta) \rho d\rho d\theta$$

where I(ρ,θ) is the point spread function of the system, ρ and θ are the polar coordinates of the image plane. K is a constant [17]. The integral of intensity point spread function in a radius allows evaluation of percent energy of the wavefront that falls within the 0th mode of the circular diffraction pattern or within the Airy disk. Figure 6(a) shows fractional encircled energy as a function of radius for transmission through a single H-PDLC. Figure 6(b) shows typical fractional encircled energy of transmission through a stack of two H-PDLC samples. Though the differences in this data are subtle, 90% of the energy falls within approximately 15% of the total beam diameter in the single H-PDLC case while 90% of the beam energy falls within approximately 20% of the total beam diameter when measuring transmitted wavefront for the stack of two H-PDLC samples. Energy spreading into the higher order diffraction rings or larger radii indicates a more aberrated wavefront.

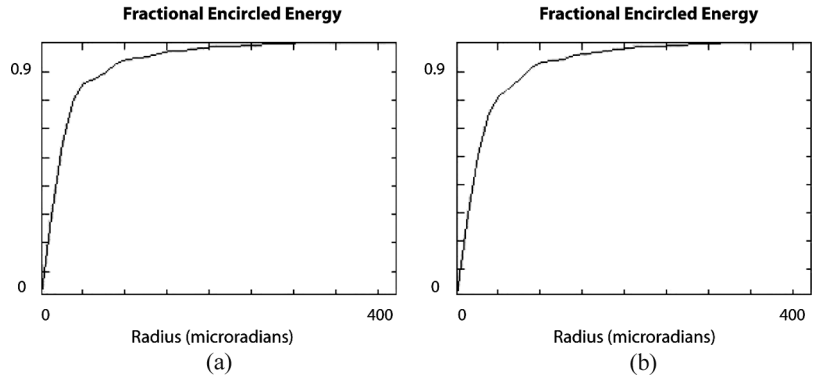

FIGURE 6 (a) Fractional encircled energy of transmission through a single H-PDLC. (b) Typical fractional encircled energy of transmission through a stack of two H-PDLC.

IV. CONCLUSIONS

In this article, we have compared several index matching fluids and optical adhesives for minimizing transmission loss between layers of H-PDLC gratings for applications relying on maximum transmission such as a thin film spectrometer. NOA65 minimized transmission loss for samples prepared on Corning 1737 glass regardless of AR-ITO or non-AR ITO coating. Additionally, transmitted wavefront has been characterized for single H-PDLC samples and stacks of two H-PDLC samples. Zernike numbers and primary aberrations were characterized for single and stacked H-PDLC samples illustrating the major primary aberrations that are visible in the reconstructed fringe pattern. H-PDLC samples stacked with NOA65 have minimized transmission loss compared to other Norland products and air gap, yet resulted in the most wavefront aberration based on Strehl ratio and primary aberration Zernike numbers. Specific choice of adhesion layer is application dependent and cannot be based solely on reduction of transmission loss. Finally, fractional encircled energy data was analyzed to illustrate that as the stack size increases, a higher percent of beam energy appears in higher order diffraction modes, indicating a more aberrated wavefront.

REFERENCES

[1] Bunning, T. J., Natarajan, L. V., Tondiglia, V. P., & Sutherland, R. L. (2000). *Annu. Rev. Mater. Sci.*, *30*, 83.

[2] Sutherland, R. L., Tondiglia, V. P., Natarajan, L. V., Bunning, T. J., & Adams, W. W. (1994). *Appl. Phys. Lett.*, *64*, 1074.
[3] Cairns, D. R., Gorkhali, S. P., Esmailzadeh, S., Vedrine, J., & Crawford, G. P. (2003). *J. SID*, *11*, 289.
[4] Date, M., Takeuchi, Y., & Kato, K. (1998). *J. Phys. D: Appl Phys.*, *31*, 2225.
[5] Meyer, F. M., Aleva, D. L., Longo, S. J., Trissell, T. L., Schwartz, R. W., & Hopper, D. G. (2002). *Proc. of SPIE*, *4712*, 373.
[6] Lucchetta, D. E., Criant, L., Francescangeli, O., & Simoni, F. (2004). *Appl. Phys. Lett.*, *84*, 4893.
[7] Hsiao, V., Lu, C., He, G., Pan, M., Cartwright, A., Prasad, P., Jakubiak, R., Vaia, R., & Bunning, T. (2005). *Opt. Ex.*, *13*, 3787.
[8] Saitoh, G., Murai, H., Uehara, S.-I., Gotoh, T., Mimura, K., Nakata, T., Sumiyoshi, K., & Hayama, H. (2001). *SID Symposium Digest, 32*, 334.
[9] Colegrove, J., Kelly, J., Fiske, T., Lewis, A., Yuan, H., Tran, H., Crawford, G. P., & Silverstein, L. (2000). *SID 00 Digest*, 770.
[10] McMurdy, J. W., Crawford, G. P., Jay, G. D., & Suner, S. (2005). *SID 05 Digest*, 364.
[11] Platt, B. C. & Shack, R. (2001). *J. Refractive Surgery*, *17*, S573.
[12] Fontecchio, A. K., Bowley, C. C., Yuan, H., & Crawford, G. P. (2001). *Molecular Crystals and Liquid Crystals*, *352*, 399.
[13] Mahajan, V. N. (1982). *J. Opt. Soc. Am*, *72*, 1258.
[14] Born, M. & Wolf, E. (1999). *Principles of Optics*, Cambridge University Press: Cambridge, UK.
[15] Wyant, J. C. & Creath, K. (1992). *Appl. Opt and Opt Engineering*, *11*, 27.
[16] Malacara, D. (1992). *Optical Shop Testing*, John Wiley & Sons, Inc.: New York.
[17] Sanyal, S. & Ghosh, A. (2002). *J. Opt. A: Pure Appl Opt.*, *4*, 208.